

# Towards Single Stage Weakly Supervised Semantic Segmentation

Peri Akiva  
Rutgers University  
peri.akiva@rutgers.edu

Kristin Dana  
Rutgers University  
kristin.dana@rutgers.edu

## Abstract

The costly process of obtaining semantic segmentation labels has driven research towards weakly supervised semantic segmentation (WSSS) methods, using only image-level, point, or box labels. The lack of dense scene representation requires methods to increase complexity to obtain additional semantic information about the scene, often done through multiple stages of training and refinement. Current state-of-the-art (SOTA) models leverage image-level labels to produce class activation maps (CAMs) which go through multiple stages of refinement before they are thresholded to make pseudo-masks for supervision. The multi-stage approach is computationally expensive, and dependency on image-level labels for CAMs generation lacks generalizability to more complex scenes. In contrary, our method offers a single-stage approach generalizable to arbitrary dataset, that is trainable from scratch, without any dependency on pre-trained backbones, classification, or separate refinement tasks. We utilize point annotations to generate reliable, on-the-fly pseudo-masks through refined and filtered features. While our method requires point annotations that are only slightly more expensive than image-level annotations, we are to demonstrate SOTA performance on benchmark datasets (PascalVOC 2012), as well as significantly outperform other SOTA WSSS methods on recent real-world datasets (CRAID, CityPersons, IAD).

## 1. Introduction

The fundamental computer vision task of semantic segmentation seeks to assign class labels to specific pixels in a given input image. The rapid development of deep learning methods has resulted in significant progress in performance [85, 17, 83, 49], stability [61, 79], and accessibility [57, 1] of semantic segmentation algorithms, often seen in real world applications such as autonomous vehicles [88, 37, 72, 12, 10, 53], precision agriculture [5, 4], medical diagnosis [82, 73, 39, 60, 67], image restoration and editing [54, 44], sports [18], and remote sensing [6, 41]. While such algorithms provide insightful information about the scene, it requires large amounts of pixel-wise labeled data [87, 48, 23], which is often expensive and time consuming to collect [9]. To alleviate this requirement, recent

efforts have focused on weakly supervised semantic segmentation (WSSS) using image-level [89, 73, 58, 3, 7, 24], center point [4, 9], scribbles [45], or bounding box [20] labels. The balance between cost and utilization is essential in determining what kind of annotations are needed. Image-level annotations may be cheap to produce, but require more complex networks not practical for real world applications. On the other hand, pixel-wise annotations may be too expensive and time consuming as an up-front cost.

The type of annotation featured in many WSSS methods is image-level labels, providing the least semantic information but are cheapest to annotate. Methods that use image-level labels often require computationally expensive methods such as multiple networks, region proposal generation, and refinement steps. These methods are often referred to as *multi-stage* weakly supervised semantic segmentation, since they include multiple stages of training and evaluation before performing final inference. Current SOTA WSSS methods utilize class activation maps (CAMs) [86, 55, 64] to obtain pixel-wise coverage and localization of objects in the scene. CAMs are often noisy, and only cover the most discriminating parts of objects, making them poor pseudo-masks candidates. For that reason, WSSS methods often resort to multiple stages of refinement before obtaining final pseudo-masks. Such *multi-stage* requirements make adapting those methods to new datasets more difficult. Any change in data distribution requires significant effort, and approaches such as online learning [13] become impractical to adapt. In this work, we aim to semantically segment images using point annotations (22.1 sec/image in annotation time compared to 20 sec/image for image-level annotations [9]) in a *single-stage* approach.

Recent work has achieved notable improvement at single-stage WSSS [7] through pseudo-mask generation and refinement to obtain comparable results with two stage methods. While resulting performance improvement is significant, the method still lacks generalizability to non-benchmark datasets due to its dependency on a pre-trained backbone. By extension, this dependency limits applicability to real world problems. Pre-trained backbones (trained on the benchmark dataset) are essentially trained classi-

fication networks, similar to what is used in multi-stage methods. They provide superior localization and coverage, “skipping” the challenging stage of generating pseudo-masks in early iterations. From our experiments, competing methods don’t generate reliable pseudo-masks without using a pre-trained network, which fundamentally loses its single stage approach when non-standard datasets are used. Performance on standard benchmark datasets is essential to determine the efficacy of novel methods. However, real world applications often necessitate segmenting scenes where image-level labels are not sufficient, e.g. pedestrian, agricultural crops, and biological cells. When images have few (or binary) object labels, classification becomes easy, the resulting coarse CAMs (from image-level labels) are enough for classification, but are insufficient for segmentation and therefore produce poor pseudo-masks. This means that dependency on a pre-trained backbone, or any image-level pre-training procedure, can be detrimental for real world applications, which we demonstrate in the experiments (table 2), results (Figure 5), and supplementary material sections.

Here, we propose a *single-stage* WSSS method that generates reliable pseudo-masks from point annotations. We choose to use point annotations since, while only costing an additional 2 seconds per image in annotation time (20.0 sec/image compared to 22.1 sec/image on average) [9], it provides spatial information essential for correctly localizing and segmenting objects. The method comprises two main novel contributions. First, a point generator component transforms few points to many points using a basic intuition: Given a user-defined object point, the task of sampling *another* object point is not so hard. In fact, classical work on random walks in image segmentation can be re-formulated for this problem. Our approach is a point augmentation by iteratively scattering the original points by small affine perturbations followed by random walks. The point-set obtained by this iterative scatter-then-walk procedure is termed *point blot*, analogous to ink blot. This point blot generation stage is entirely deterministic and does not require any training. Furthermore, the resulting point blot has significantly more utility compared to the original point-clicks. The second contribution in our framework is the *expanding distance fields*, a new instantiation of the classic distance fields [14] that is refined within the learning pipeline to capture changing inter-class distances. When considering early training iterations of an un-trained network, outputs are expected to be noisy and unstable, producing unreliable pseudo-masks. To mitigate such errors, we employ pixel adaptive convolution refinement network along with our expanding distance fields. The former rectifies locally inconsistent regions conditioned to local statistical representation, and the latter filters wrongly activated regions, and stabilizes training by preventing accu-

mulation of bias in generated pseudo-masks. Our main contribution is a method to generate pseudo-masks from points that use point blot generation and expanding distance fields. Notably, our method eliminates the dependency on pre-trained backbones and classification tasks for WSSS. We achieve SOTA performance on single-stage WSSS. We achieve significantly better performance in non-benchmark datasets from important application domains.

## 2. Related Work

### 2.1. Semantic Segmentation

Semantic segmentation is a dense image prediction task that predicts class labels for every pixel in a given image. The quick progress in deep learning and convolutional neural networks [35, 66, 69, 30] has powered the development of the fully convolutional network (FCN) [49], which is the basis to many current SOTA semantic segmentation methods [85, 17, 83, 61]. Typical design of semantic segmentation networks utilize encoder-decoder architectures, in which deep features are learned, and up-sampled to match the input image size. More recent work improve this base design by incorporating skip connections [61], contextual information [83], self-attention mechanisms [25], enlarged receptive fields [85, 29], pyramid pooling [85, 17, 29, 47], and refiner networks [46]. U-Net [61] adopts skip connections to fuse information from low level layers into high level layers. PSPNet [85] features a multi-scale pyramid pooling module applied to sub-regions that act as the contextual representation of that region. A similar type of pyramidal pooling scheme is employed in DeepLap [17] and Feature Pyramid Networks (FPN) [47]. EncNet [83] encodes multi-scale contextual features using a Gaussian kernel. With similar goals in mind, ASPP [29] captures additional contextual information through dilated convolution layers, which enlarge the receptive field of the layer without added parameters. While those networks often provide SOTA performance, they still require expensive computational cost and fully supervised ground truth.

### 2.2. Class Activation Maps and Region Proposals

The activated neurons of a deep learning network with response to an input image are called class activation maps (also referred to as CAMs or attention maps) [86]. They represent regions the network finds most distinctive for a given class label. Initial work leveraging CAMs were used for object localization [55, 86, 70, 11, 42] and network interpretability [64], but were recently adopted for semantic and instance segmentation tasks [25, 3, 73, 24, 16, 89]. Most approaches utilize CAMs as masks, region proposals, or auxiliary data used to generate labels for segmentation methods. Since CAMs tend to be noisy and irregular in shape, much focus in the WSSS domain has been devoted towards refining outputs to improve CAM coverage accuracy and consistency. SEAM [75] addresses the volatility of CAM out-

puts by enforcing consistency between transformed inputs using a siamese network. Instead of learning better CAMs, SSDD [65] resorts to two post-processing refinement networks (also read as two additional stages) to improve outputs before generating pseudo-masks.

### 2.3. Weakly Supervised Semantic Segmentation

The majority of work done in the WSSS domain is accomplished in a multi-step process: train a classification or segmentation network, apply the network on the training set to extract CAMs, which are then refined and thresholded before used to train a separate segmentation network. Early work like BoxSup [20] utilize bounding boxes to update pre-defined region proposals to generate ground truth masks for the training set. AffinityNet [3] leverages image level labels to generate affinity labels obtained through selection of high confidence points on amplified CAMs. Similarly, PRM (Peak Response Map) [89] back-propagates through local extrema points in attention maps to generate instance-wise pseudo-masks. Additional methods [73, 24, 16, 33, 75, 40] follow a similar approach using image level labels for pseudo-mask generation. While those methods achieve significant performance improvement over previous weakly supervised methods, they all utilize ground truth labels during inference time to eliminate activation maps of classes not present in the image. That practice is consistent with the *multi-stage* process of acquiring pseudo-masks for the training set, during which labels are assumed to be present.

Recent single stage WSSS methods [4, 7, 33, 31, 32, 56, 58, 63] are less common due to the challenge of implicitly obtaining reliable spatial and contextual information from weak labels. Triple-S [4] uses point supervision and shape priors as spatial and contextual cues for the network. However, the use of shape priors is highly restrictive, and explicitly provides spatial and contextual information to the network, making the method too task specific. In contrast, Araslanov *et al.* [7] train a segmentation-aware classification network using normalized global weighted pooling (nGWP), iterative mask refinement, and focal mask penalty. Normalized global weighted pooling allows concurrent classification and segmentation training, while the output mask prediction is iteratively refined using Pixel Adaptive Convolution (PAC) layers introduced in [68]. While [7] shows significant improvement in single stage WSSS, the method requires a pre-trained backbone to achieve good performance. The use of pre-trained weights removes biases and randomness present during initial training steps, allowing for superior pseudo-mask generation. Generally, as seen in [55, 64], a trained classification network provides “free” localization of the objects by locating peaks in class activation maps. Such localization would not be available unless the backbone is pre-trained, or trained first. Since [7] requires training a classification network as an addi-

tional stage, then it may be considered a two-stage approach when used for non-benchmark datasets. Similar to [7], we also adopt our own version of Pixel Adaptive Convolution layers [68] for feature refinement, and subsequent pseudo-mask generation.

## 3. Pseudo-Masks from Points

The motivation behind our method is to obtain reliable, on-the-fly pseudo-masks from initial points to train a semantic segmentation network. Intuitively, the better the ground truth labels, the better the network’s performance. Pseudo-masks are typically obtained through some thresholding of high confidence (high activation) features. When training from scratch, such features tend to be noisy, and directly thresholding such features will generate poor pseudo-masks which will result in sub-optimal training and performance. We address that challenge by using the Expanding Distance Fields module (section 3.2), which filters wrongly activated regions, and captures and amplifies correctly activated regions. It also introduces a new aggregation approach and expansion mechanism that alleviates overfitting to features around ground truth points. We also employ a Point Blot Generator (section 3.3) and its point blot output to provide superior utility compared to points alone, capturing additional locally available contextual information, and accelerating training progress. As seen in Figure 1, we incorporate a feature refinement network (section 3.1) to work in tandem with our Expanding Distance Fields to produce intermediate pseudo-masks, which are superimposed with point blots to make the final pseudo-masks for supervision.

### 3.1. Pixel Adaptive Convolution Refinement Network

Our implementation of Pixel Adaptive Convolution Refinement Network (also referred to as PAC Refinement Network or PAC Refiner) stems from pixel adaptive convolution layers [68]. They allow for dynamic modification of kernel weights based on some underlying conditions, and are commonly used in feature refinement work [76, 38, 22, 81, 71, 7] with modified kernel functions. Here, we use PAC layers to dampen activated regions in the output features that are not locally consistent. Our PAC Refinement Network considers the local standard deviation of the input image in color space and the local mean in feature space to amplify output regions with low standard deviation and high mean. Given network output  $\tilde{x}$  and its corresponding softmax  $\tilde{x}_s$ , we feed  $\tilde{x}_s$  to an  $L$  layer network consisting of pixel adaptive convolution layers with kernel  $k$  as a function of the corresponding pixel values in  $X$  and features in  $\tilde{x}_s^{(l-1)}$  (the output of previous layer in the PAC refinement network), where  $l$  is the current layer. More specifically,

$$\tilde{x}_s^l = \tilde{x}_s^{(l-1)} \circledast k,$$

where

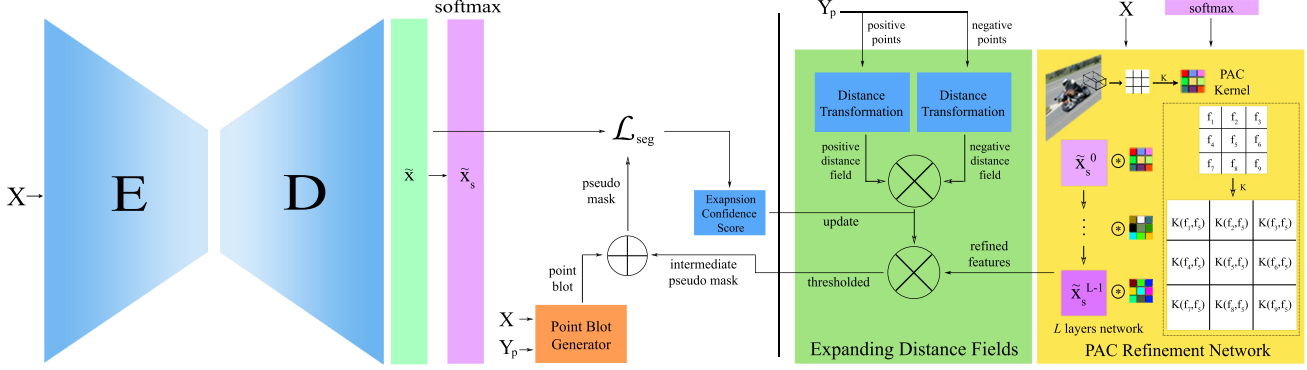


Figure 1: **Pseudo-Mask from Points (PMP)** overall architecture. Input image is fed to a fully convolutional network, and supervised by a pseudo-mask generated by the Expanding Distance Fields (*green box*) and Point Blot Generation (*orange box*) modules. The network’s output features is refined with accordance to local statistics of underlying features and color distributions using our Pixel Adaptive Convolution Refinement Network variant (*yellow box*). The refined features are then multiplied element-wise with expanded distance fields to generate intermediate pseudo-masks. When training a network from scratch, early iterations tend to be unstable, producing noisy outputs and therefore unreliable pseudo-masks. Our novel Expanding Distance Fields allow from-scratch training by preventing accumulation of error in generated pseudo-masks. Best viewed in color and zoomed.

$$k_{i,j} = -\frac{|X_{i,j} - X_{l,n}|}{\sigma_{i,j}} \mu_{i,j}.$$

$(i, j)$  correspond to the current location of the kernel,  $(l, n)$  are all neighboring pixels of  $(i, j)$ ,  $\tilde{x}_s^{(l-1)}$  is the output of the previous PAC Refiner layer,  $\sigma_{i,j}$  is the standard deviation of the current kernel region in  $X$ , and  $\mu_{i,j}$  is the mean value of the current kernel region in  $\tilde{x}_s^{(l-1)}$ . Note that  $X$  is normalized between 0-1.

Consider a region over an edge, in which we can expect a larger standard deviation in color intensity, which will result in a smaller kernel weight (dampening kernel). Similarly, the mean over the kernel region in feature space depicts both local similarity and relevancy of those pixels. Low similarity and/or relevancy will reduce the kernel weight over that region. When applied over the entire image, we dampen all locally inconsistent activated regions in  $\tilde{x}_s$ . The overall operation is structured as an  $L$  pixel-adaptive convolution layer network with varying kernel sizes, dilations, and strides. Note that since kernel weights are functions of local color and feature statistical representation (standard deviation and mean), the refined features are the output of a single forward pass of the network. There are no learned weights in this operation, making it computationally inexpensive.

### 3.2. Expanding Distance Fields

Expanding Distance Fields aim to impose global consistency and correct localization in the refined feature space (obtained from 3.1) by leveraging background (negative) and object (positive) point annotations to generate distance fields (section 3.2.1). These distance fields are then updated by our expansion mechanism (section 3.2.2) which allows the distance field to incrementally incorporate more refined features into the final output.

#### 3.2.1 Distance Field Aggregation

The use of distance fields [14] is common in interactive segmentation methods [26, 62, 27, 28, 8, 43, 80, 52, 34], where it is used as auxiliary data produced from user inputs such as points and scribbles. Here, we use it as a point-guided filter to enforce object localization consistency in the refined features and subsequent generated pseudo-masks. Our usage of distance fields filters is essential in stabilizing training in early iterations, during which output features lack sound structure to make reliable pseudo-masks. Distance fields are computed by taking the minimum Euclidean distance between a given point and the rest of points present in the scene. Given image  $X \in \mathcal{R}^{H \times W \times 3}$  and ground truth points  $Y_p \in \mathcal{R}^{H \times W \times 1}$ , where  $Y_p(i, j) \in \{0, 1, \dots, C+1\}$  (label  $C+1$  represents background points), we use  $Y_p$  to obtain class-wise distance fields  $D \in \mathcal{R}^{(C+1) \times H \times W}$ , where  $C$  is the number of classes. For example, to generate a distance field  $D_c$  for some class  $c$ , we compute the value of  $D(c, i, j)$  at location  $(i, j)$  using  $D(c, i, j | Y_p) = \min \sqrt{(i - p_{c,i})^2 + (j - p_{c,j})^2}$ , where  $p_c$  is a point in  $Y_p$  that belongs to class  $c$  (also referred to as positive points). We repeat this for every point and class in the image to obtain  $D \in \mathcal{R}^{(C+1) \times H \times W}$ , including for background (or negative) points. Typically, such distance fields are concatenated to the input image of interactive segmentation methods. Instead, we leverage the distance fields to enforce object localization consistency on intermediate pseudo-masks. We invert the normalized background distance field  $D_{C+1}$ , and perform element-wise multiplication with all other distance maps:  $D_c = (1 - D_{C+1}) \odot D_c \forall c \in \{1, \dots, C\}$ . Inverting  $D_{C+1}$  imposes low values in regions known to belong to the background class. By taking the element-wise product between  $D_{C+1}$  and all other distance maps, we remove regions in  $D_c$  that may be ambiguous or inconsis-

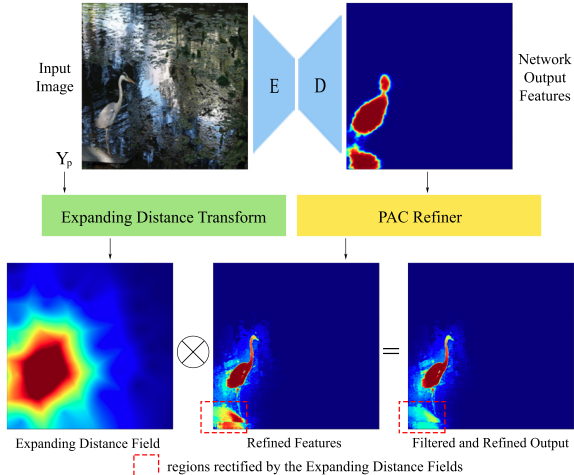


Figure 2: **Expanding Distance Fields and PAC Refinement Network** joint utility example on Pascal VOC 2012 [23]. The network output features are fed to the PAC Refiner, which output is multiplied element-wise with the expanding distance fields obtained from point annotations and expansion confidence score. Observe that the rock is wrongly activated for the bird class, which is dampened by the expanding distance field. The regions highlighted by the red dash boxes indicate wrongly activated regions and their dampened outputs. The final output is thresholded to make the intermediate pseudo-mask. Epoch-by-epoch progress of pseudo-masks, refined features, and expanding distance fields is available in the supplementary material. Best viewed in color and zoomed.

tent with the underlying object’s location. This can also be observed in Figure 2, where the wrongly activated region (marked with a red box) is dampened by the distance field.

### 3.2.2 Expansion Mechanism

Using points as seeds to create distance fields inherently creates bias towards the regions around those seeds, especially when objects are large. For that reason, we employ our novel expansion mechanism, which aims to represent increasing dependability of the model on the refined features. Typically, outputs tend to be noisy in early training iterations, and as training progresses we expect better output feature representations. If the distance fields are used alone without the expansion mechanism, the intermediate pseudo-masks tend to provide partial coverage for images with large objects. Instead, we define an expansion confidence score,  $\mathcal{E}_{score}$ , which is a function of the network’s learning progress. In initial stages of training, we consider the seed point as the pixel with highest confidence, corresponding to the value of 1. As the network learns features corresponding to that class, we incrementally lower the highest confidence threshold. By doing so, we expand the distance field from the seed point outward, essentially enlarging the region of high confidence and allowing more refined features in to be included in the output. If done

indefinitely, the generated refined features will be “fully trusted,” meaning the entirety of the refined features will be included in the output. Formally,

$$\gamma = \frac{\mathcal{L}^{(e-1)}}{\mathcal{L}^{(e)}} - 1,$$

$$\mathcal{E}_{score} = \mathcal{E}_{score} + \max(\min(\gamma, \eta), \omega),$$

where  $\mathcal{L}^{(e)}$  is the accumulated loss at epoch  $e$ ,  $\gamma$  is the improvement ratio between the current and previous epochs, and  $\eta$  and  $\omega$  are the upper and lower limits for confidence improvements to be added to  $\mathcal{E}_{score}$  at that epoch. Note that performance degradation at a given epoch will result in a lower confidence score for the next epoch. We use the confidence score to modify our distance map aggregation by adding it to the distance fields, and clipping any values below 0 and above 1 as follows,

$$\mathcal{D}_{c,x,y} = \begin{cases} 1 & \text{if } \mathcal{D}_{c,x,y} + \mathcal{E}_{score} \geq 1 \\ 0 & \text{if } \mathcal{D}_{c,x,y} + \mathcal{E}_{score} \leq 0 \\ \mathcal{D}_{c,x,y} + \mathcal{E}_{score} & \text{otherwise} \end{cases}$$

where  $x$  and  $y$  represent all possible locations of distance field for class  $c$ . Classes not present in the image are ignored. Note that we use different expanding confidence scores for the background and the objects, and the object expanding scores increase 2 times faster than the background expanding score. The importance of this module is also visually demonstrated in the supplementary material through epoch-by-epoch distance field instances and their corresponding pseudo-masks.

**The final step** of the Expanding Distance Fields module performs an element-wise product between the refined features and the aggregated distance fields, followed by thresholding, to obtain the final pseudo-mask. Since the PAC refinement network only smooths and ensures local consistency, without global perspective, it often has activated regions that are not part of the objects. By multiplying its output with the aggregated distance fields, we spatially constrain the class activation maps to regions determined to be relevant by the distance fields. This is visually demonstrated in Figure 2 which shows the transition between each stage up to the final pseudo-mask.

### 3.3. Point Blot Generator

The purpose of this method is to generate a set of new local ground truth pixels from image  $X$ , and annotated points  $Y_p$  through iterative operations of perturbations and random walks over the input image  $X$ . The set of new ground truth pixels, named point blots, capture neighboring pixels that are “obviously” part of the object. Such additional pixels are essential in the early iterations because they provide reliable baseline pseudo-masks before the network is able to generate meaningful features. The role of these point blots

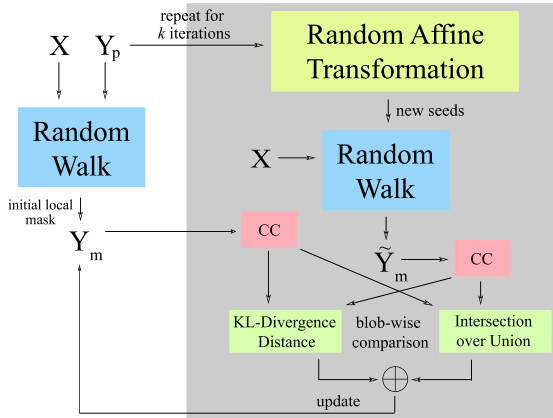


Figure 3: **Point Blot Generator** pipeline. The module generates initial point blots using input image and ground truth points. Initial point blots are then iteratively updated conditioned to coverage matching and underlying color distribution similarity of current and candidate blobs. Candidate blobs are generated through perturbations of initial points followed by random walks in color space, which are then separated into candidate blobs using the connected component algorithm [21] (noted as CC).

decreases as the intermediate pseudo-mask generated by the PAC Refiner and Expanding Distance Fields improve.

Let image  $X \in \mathcal{R}^{H \times W \times 3}$  and ground truth points  $Y_p \in \mathcal{R}^{H \times W \times 1}$  be an input sample to the Point Blot Generation module. We obtain an initial mask,  $Y_m$ , using a random walk over  $X$  with  $Y_p$  as seeds. Then, we perturb  $Y_p$  using a random affine transformation to obtain new points  $\tilde{Y}_p$ , which are used as seeds for a random walk over  $X$  to generate a candidate mask  $\tilde{Y}_m$ . While we can guarantee that all points in  $Y_p$  lay on the correct objects, we cannot assume the same for  $\tilde{Y}_p$ , and consequently cannot assume that  $\tilde{Y}_m$  is a good candidate mask as a whole. Instead, we partition  $Y_m$  and  $\tilde{Y}_m$  into current and candidate blobs,  $B, \tilde{B}$ , using the connected component algorithm [21], with each current blob  $b \in B$  corresponding to a candidate blob  $\tilde{b} \in \tilde{B}$ . We then calculate the Kullback–Leibler divergence (KLD) distance [36] between the distributions of the underlying image features enclosed by the pixels of  $b$  and  $\tilde{b}$ . A candidate blob is accepted as an expansion to its corresponding current blob if it fulfils two requirements: 1) the KLD distance is smaller than threshold  $\phi$ , and 2) the intersection over union of  $b$  and  $\tilde{b}$  is above threshold  $\delta$ . This set of perturbations is repeated for  $k$  iterations with increasing perturbation intensity, in which random affine transformations sample from increasing ranges of rotations and translations. The KLD distance ensures that color intensity distribution of pixels in blobs are similar to each other, while the intersection over union threshold requires that we expand gradually, without creating disjoint blobs. The increased perturbations also ensure that we first explore neighboring regions to obtain suc-

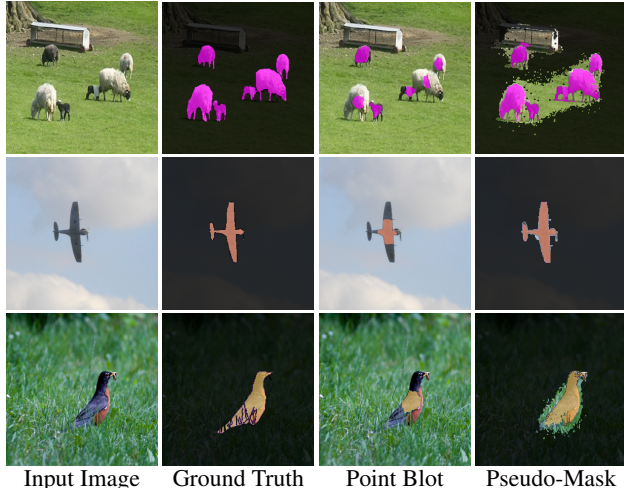


Figure 4: **Qualitative results** of our generated pseudo-masks and point blots on Pascal VOC [23] training set. Our method provides pseudo-masks converging towards fully-supervised ground truth, allowing for better performance, even when training from scratch. Pixels with low certainty (not color coded) are ignored. Dark gray pixels represent background class. Best viewed in color and zoomed.

cessive expansion.

The point blot generation pipeline can be seen in Figure 3, and output samples in Figure 4. The method allows us to capture additional neighboring pixels around points without sacrificing excessive computation resources, increasing computational time per iteration by roughly 9.42%.

## 4. Experiments

We train and evaluate the performance of our method on four datasets: Pascal VOC 2012 [23], Cranberry from Aerial Imagery Dataset (CRAID) [4], CityPersons [84, 19], and Inria Aerial Dataset (IAD) [51]. The first is to illustrate our method’s performance on a standard benchmark dataset, and the rest are examples of real world applications. While standard benchmark datasets are essential for baseline efficacy assessment, we want to demonstrate our method’s generalizability and flexibility in domains more common in real world applications. We select the CRAID, CityPersons, and IAD datasets because they provide point annotations (up-front or through a pre-processing step) for objects and backgrounds and fully supervised evaluation sets. Pascal VOC 2012 dataset contains 12,031 images, with 10,582 used for training, and 1,449 for validation. We obtain points for objects by selecting the center points of bounding boxes, and points for backgrounds by uniformly sampling four points per object outside of all boxes in a given scene. Since the center points of objects may not always be located on the object, creating bias in our ground truth, we believe that our method will work even better with datasets that were annotated using points.

For our real world examples, CRAID [4], a compu-

Dataset	Pascal VOC 2012 [23]		
Method	Supervision	val	test
<i>Single Stage, Full Supervision</i>			
WideResNet38 [79]	$\mathcal{F}$	80.8	82.5
DeepLab v3 [17]	$\mathcal{F}$	-	87.8
<i>Multi Stage + Saliency</i>			
Bearman <i>et al.</i> [9]	$\mathcal{S}, \mathcal{P}$	46.0	43.6
MDC [77]	$\mathcal{S}, \mathcal{I}$	60.4	60.8
MCOF [74]	$\mathcal{S}, \mathcal{I}$	60.3	61.2
DSRG [33]	$\mathcal{S}, \mathcal{I}$	61.4	63.2
BoxSup [20]	$\mathcal{S}, \mathcal{B}$	62.0	64.6
CIAN [24]	$\mathcal{S}, \mathcal{I}$	64.1	64.7
FickleNet [40]	$\mathcal{S}$	64.9	65.3
<i>Multi Stage</i>			
AffinityNet [3]	$\mathcal{I}$	61.7	63.7
IRNet [2]	$\mathcal{I}$	63.5	64.8
SSDD [65]	$\mathcal{I}$	64.9	65.5
SEAM [75]	$\mathcal{I}$	64.5	65.7
<i>Single Stage</i>			
EM [56]	$\mathcal{I}$	38.2	39.6
MIL-LSE [58]	$\mathcal{I}$	42.0	40.6
CRF-RNN [63]	$\mathcal{I}$	52.8	53.7
Araslanov <i>et al.</i> [7]	$\mathcal{I}$	59.7	60.5
Araslanov <i>et al.</i> + CRF [7]	$\mathcal{I}$	62.7	64.3
Ours	$\mathcal{P}$	60.7	60.8
Ours + CRF	$\mathcal{P}$	62.9	63.8

Table 1: mIoU (%) accuracy (higher is better) on Pascal VOC 2012 validation and test sets [23].  $\mathcal{F}$ ,  $\mathcal{I}$ ,  $\mathcal{B}$ ,  $\mathcal{S}$ , and  $\mathcal{P}$  represent full, image, box, saliency, and point level annotations respectively. Our method achieves SOTA performance even with from-scratch training. Class-wise performance is available in supplementary material.

tational agriculture dataset, provides 1022 images with point annotations, and 231 with pixel-wise annotations, CityPersons [84], a pedestrian detection dataset subset of Cityscapes [19], provides 2115 training and 391 testing image with bounding boxes (processed to points similar to Pascal VOC), and IAD [51], a remote sensing dataset, provides 180 images (cropped to 29239 images) with pixel-wise annotations (processed to points).

#### 4.1. Implementation Details

To highlight the contribution of our method, we choose to adopt a standard fully convolutional network (*untrained* ResNet50 backbone encoder) that is trained from scratch. Note that this is not typical of other baseline methods, in which pre-trained, complex networks (often pre-trained on the benchmark or similar dataset) are used to achieve SOTA performance. Our network is trained using the SGD op-

Dataset	CRAID [4]	CityPersons [84]	IAD [51]
Method	Sup.	mIoU (%)	
DeepLab v3 [17]	$\mathcal{F}$	81.3	80.7
ICT-Net [15]	$\mathcal{F}$	-	-
Araslanov <i>et al.</i> [7]	$\mathcal{I}$	54.9	48.2
Triple-S [4]	$\mathcal{P}, \mathcal{D}$	68.7	-
Ours	$\mathcal{P}$	<b>72.1</b>	<b>62.8</b>

Table 2: mIoU (%) accuracy on CRAID [4], CityPersons [84], and IAD [51] test sets. Our method is generalizable to arbitrary datasets, significantly outperforming our single-stage baselines on the selected real world datasets.

timizer, with starting learning rate of 1e-5 and cosine annealing scheduler [50]. We use weight standardization [78] and group normalization layers [59] with group size of 32. Training data is augmented with normalization transformation, color jittering, and random vertical and horizontal flips. We use Cross Entropy loss for training, with “0” labels ignored (background points, labeled as  $\mathcal{C} + 1$ , are considered instead). For the PAC Refinement Network, we use 12 layers with kernel sizes (7, 7, 5, 5, 3, 3, 3, 3, 3, 3, 3), dilations (1, 1, 2, 2, 4, 4, 8, 8, 16, 16, 32, 32), and strides (2, 2, 2, 2, 1, 1, 1, 1, 1, 1, 1, 1). We use  $-0.025, 0.025$  for lower and upper limits for the Expanding Distance Fields, and 0.75 for pseudo-mask thresholding. For performance evaluation, we report mean Intersection over Union (mIoU) for both validation and test sets. Note that all experiments reported in the main paper are done in a single stage, without pruning or eliminating output predictions. Baseline method for real world datasets was trained in accordance with the method’s reported procedure.

## 5. Results

Table 1 presents comparisons between SOTA baselines and our method on the Pascal VOC dataset. In the single-stage approach, our base method outperforms [7] by 1% on validation and 0.3% on test sets, even though we train our network from scratch and [7] uses a pre-trained backbone. It is important to note that, as shown in [86, 64, 55], localization is “free” when a trained classification network (i.e. pre-trained backbone) is available, which serves a similar role to our ground truth points. From our experiments, without the usage of a pre-trained backbone, [7] performs significantly worse. On the other hand, using points removes the necessity of separately train a classification network or use pre-trained weights, allowing our method to be used in a broader context and on non-standard datasets without incurring significant additional annotation costs. Table 2 demonstrates the wider range of the capabilities of our method, which performs significantly better than the single-stage baseline ([7]) on the CRAID, CityPersons, and IAD datasets. The poor performance of [7], or other image-level label driven methods, stems from the dependency on the preceding classification task to provide good class activa-

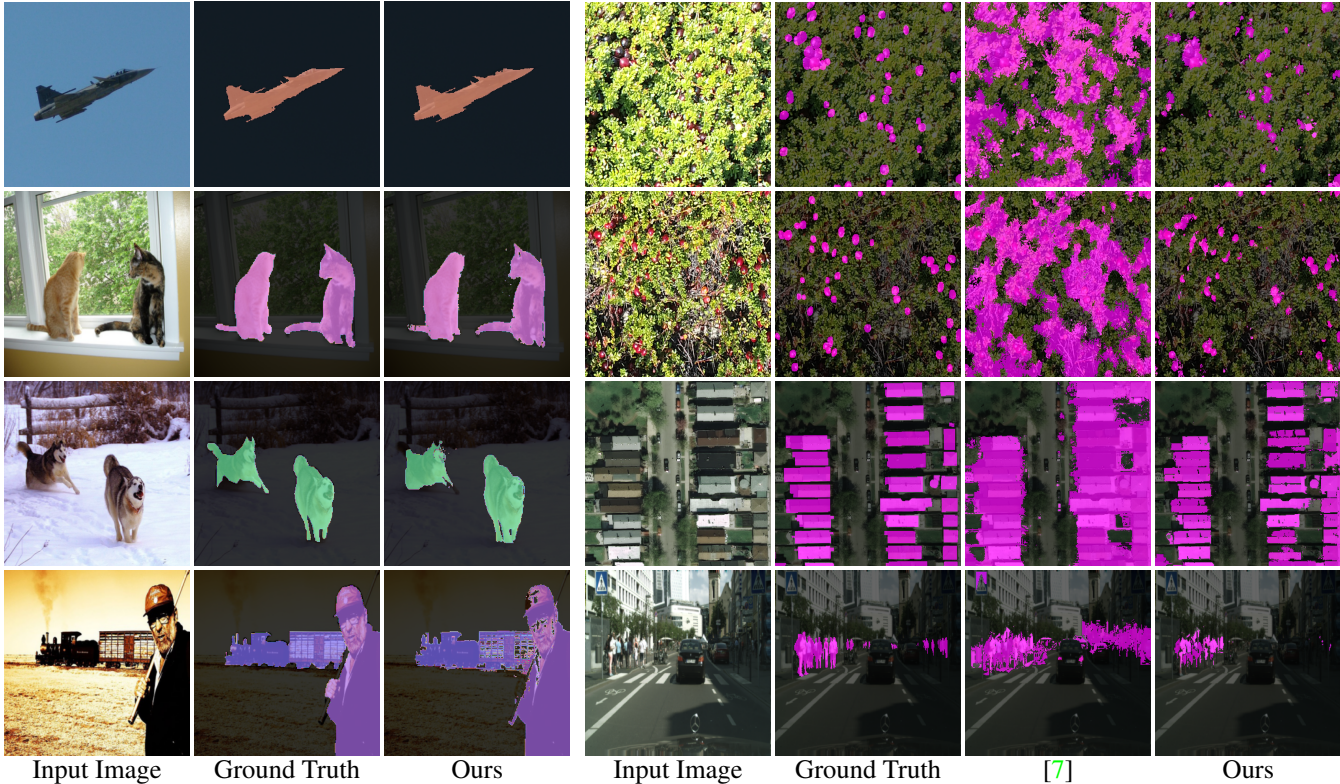


Figure 5: **Qualitative results** of our method on Pascal VOC 2012 [23] (left), CRAID [4] (right, first two rows), IAD [51] (right, third row), and CityPersons [84, 19] (right, last row) trained with points. Observe that our method provides significantly more refined predictions than our single-stage baseline (trained on image-level) on real world datasets (right side). Best viewed in color and zoomed. Dark gray pixels represent background class.

Expanding Distance Fields	Point Blot	PAC Refiner	mIoU (%)
	<i>points only</i>		15.2
	✓	✓	24.7
	✓		49.1
✓			38.3
✓	✓		48.9
✓		✓	54.5
✓	✓	✓	<b>60.7</b>

Table 3: **Ablation study** on Pascal VOC 2012 validation set [23]. We investigate the effects of each component in our proposed method and show its impact on overall performance. We consider five variations of our modules with their respective performance shown above. Note when point blots are not used, points are used instead. If PAC Refiner or Expanding Distance Fields is used, then pseudo-mask is generated from thresholded output (refined or not) features. It can be seen from the result that thresholding refined features alone is not enough, and that spatially accurate features obtained by the expanding distance fields are essential in generation of better pseudo-masks and performance.

tion maps essential for localization. When the images have few (or binary) classes, the classification becomes too easy which results in less refined feature outputs and sub-optimal localization and CAM coverage. The effects of such depen-

dencies are greatly magnified with respect to the number of objects in the scene, making scenes such as in CRAID and CityPersons, which have large counts of small objects, increasingly difficult for any method using image-level labels for segmentation. This can also be observed in the qualitative results, with our baseline producing coarse outputs for CRAID and CityPersons datasets. In contrary, images in Pascal VOC 2012 have an average of 2.37 objects per image, making it easier to generate features without spatial guidance. Thorough empirical analysis of performance degradation with decrease in object sizes and increase in counts is explained in [89]. Additional class-wise quantitative results of our method and the baselines for Pascal VOC 2012 and qualitative results for CRAID, CityPersons, and IAD datasets are available in the supplementary material.

## 5.1. Conclusion

This paper presents a practical single-stage weakly supervised semantic segmentation method applicable to non-standard datasets for which pre-trained backbones are not available, or pre-training classification task is insufficient. By utilizing our expanding distance fields and point blots, our method is able to achieve SOTA performance on the benchmark dataset as well as significantly better performance than SOTA methods on real-world domains.



## References

- [1] Martín Abadi, Ashish Agarwal, Paul Barham, Eugene Brevdo, Zhifeng Chen, Craig Citro, Greg S. Corrado, Andy Davis, Jeffrey Dean, Matthieu Devin, Sanjay Ghemawat, Ian Goodfellow, Andrew Harp, Geoffrey Irving, Michael Isard, Yangqing Jia, Rafal Jozefowicz, Lukasz Kaiser, Manjunath Kudlur, Josh Levenberg, Dandelion Mané, Rajat Monga, Sherry Moore, Derek Murray, Chris Olah, Mike Schuster, Jonathon Shlens, Benoit Steiner, Ilya Sutskever, Kunal Talwar, Paul Tucker, Vincent Vanhoucke, Vijay Vasudevan, Fernanda Viégas, Oriol Vinyals, Pete Warden, Martin Wattenberg, Martin Wicke, Yuan Yu, and Xiaoqiang Zheng. TensorFlow: Large-scale machine learning on heterogeneous systems, 2015. Software available from tensorflow.org. **1**
- [2] Jiwoon Ahn, Sunghyun Cho, and Suha Kwak. Weakly supervised learning of instance segmentation with inter-pixel relations. In *Proceedings of the IEEE/CVF Conference on Computer Vision and Pattern Recognition*, pages 2209–2218, 2019. **7**
- [3] Jiwoon Ahn and Suha Kwak. Learning pixel-level semantic affinity with image-level supervision for weakly supervised semantic segmentation. In *Proceedings of the IEEE Conference on Computer Vision and Pattern Recognition*, pages 4981–4990, 2018. **1, 2, 3, 7**
- [4] Peri Akiva, Kristin Dana, Peter Oudemans, and Michael Mars. Finding berries: Segmentation and counting of cranberries using point supervision and shape priors. In *Proceedings of the IEEE/CVF Conference on Computer Vision and Pattern Recognition Workshops*, pages 50–51, 2020. **1, 3, 6, 7, 8**
- [5] Peri Akiva, Benjamin Planche, Aditi Roy, Kristin Dana, Peter Oudemans, and Michael Mars. Ai on the bog: Monitoring and evaluating cranberry crop risk. In *Proceedings of the IEEE/CVF Winter Conference on Applications of Computer Vision (WACV)*, pages 2493–2502, January 2021. **1**
- [6] Peri Akiva, Matthew Purri, Kristin Dana, Beth Tellman, and Tyler Anderson. H2o-net: Self-supervised flood segmentation via adversarial domain adaptation and label refinement. In *Proceedings of the IEEE/CVF Winter Conference on Applications of Computer Vision (WACV)*, pages 111–122, January 2021. **1**
- [7] Nikita Araslanov and Stefan Roth. Single-stage semantic segmentation from image labels. In *Proceedings of the IEEE/CVF Conference on Computer Vision and Pattern Recognition*, pages 4253–4262, 2020. **1, 3, 7, 8**
- [8] Junjie Bai and Xiaodong Wu. Error-tolerant scribbles based interactive image segmentation. In *Proceedings of the IEEE Conference on Computer Vision and Pattern Recognition*, pages 392–399, 2014. **4**
- [9] Amy Bearman, Olga Russakovsky, Vittorio Ferrari, and Li Fei-Fei. What’s the point: Semantic segmentation with point supervision. In *European conference on computer vision*, pages 549–565. Springer, 2016. **1, 2, 7**
- [10] Matteo Bassetton, Umberto Michieli, Gianluca Agresti, and Pietro Zanuttigh. Unsupervised domain adaptation for semantic segmentation of urban scenes. In *Proceedings of the IEEE/CVF Conference on Computer Vision and Pattern Recognition (CVPR) Workshops*, June 2019. **1**
- [11] Hakan Bilen and Andrea Vedaldi. Weakly supervised deep detection networks. In *Proceedings of the IEEE Conference on Computer Vision and Pattern Recognition*, pages 2846–2854, 2016. **2**
- [12] Hermann Blum, Paul-Edouard Sarlin, Juan Nieto, Roland Siegwart, and Cesar Cadena. Fishyscapes: A benchmark for safe semantic segmentation in autonomous driving. In *Proceedings of the IEEE/CVF International Conference on Computer Vision (ICCV) Workshops*, Oct 2019. **1**
- [13] Léon Bottou. Online algorithms and stochastic approximations. *Online learning and neural networks*, 1998. **1**
- [14] Heinz Breu, Joseph Gil, David Kirkpatrick, and Michael Werman. Linear time euclidean distance transform algorithms. *IEEE Transactions on Pattern Analysis and Machine Intelligence*, 17(5):529–533, 1995. **2, 4**
- [15] Bodhiswata Chatterjee and Charalambos Poullis. Semantic segmentation from remote sensor data and the exploitation of latent learning for classification of auxiliary tasks. *arXiv preprint arXiv:1912.09216*, 2019. **7**
- [16] Arslan Chaudhry, Puneet K Dokania, and Philip HS Torr. Discovering class-specific pixels for weakly-supervised semantic segmentation. *arXiv preprint arXiv:1707.05821*, 2017. **2, 3**
- [17] Liang-Chieh Chen, George Papandreou, Iasonas Kokkinos, Kevin Murphy, and Alan L Yuille. Deeplab: Semantic image segmentation with deep convolutional nets, atrous convolution, and fully connected crfs. *IEEE transactions on pattern analysis and machine intelligence*, 40(4):834–848, 2017. **1, 2, 7**
- [18] Anthony Cioppa, Adrien Deliege, Maxime Istasse, Christophe De Vleeschouwer, and Marc Van Droogenbroeck. Arthus: Adaptive real-time human segmentation in sports through online distillation. In *Proceedings of the IEEE/CVF Conference on Computer Vision and Pattern Recognition (CVPR) Workshops*, June 2019. **1**
- [19] Marius Cordts, Mohamed Omran, Sebastian Ramos, Timo Rehfeld, Markus Enzweiler, Rodrigo Benenson, Uwe Franke, Stefan Roth, and Bernt Schiele. The cityscapes dataset for semantic urban scene understanding. In *Proc. of the IEEE Conference on Computer Vision and Pattern Recognition (CVPR)*, 2016. **6, 7, 8**
- [20] Jifeng Dai, Kaiming He, and Jian Sun. Boxesup: Exploiting bounding boxes to supervise convolutional networks for semantic segmentation. In *Proceedings of the IEEE International Conference on Computer Vision*, pages 1635–1643, 2015. **1, 3, 7**
- [21] Michael B Dillencourt, Hanan Samet, and Markku Tamminen. A general approach to connected-component labeling for arbitrary image representations. *Journal of the ACM (JACM)*, 39(2):253–280, 1992. **6**
- [22] Aysegul Dundar, Karan Sapra, Guilin Liu, Andrew Tao, and Bryan Catanzaro. Panoptic-based image synthesis. In *Proceedings of the IEEE/CVF Conference on Computer Vision and Pattern Recognition*, pages 8070–8079, 2020. **3**

- [23] M. Everingham, L. Van Gool, C. K. I. Williams, J. Winn, and A. Zisserman. The pascal visual object classes (voc) challenge. *International Journal of Computer Vision*, 88(2):303–338, June 2010. 1, 5, 6, 7, 8
- [24] Junsong Fan, Zhaoxiang Zhang, Tieniu Tan, Chunfeng Song, and Jun Xiao. Cian: Cross-image affinity net for weakly supervised semantic segmentation. In *Proceedings of the AAAI Conference on Artificial Intelligence*, volume 34, pages 10762–10769, 2020. 1, 2, 3, 7
- [25] Jun Fu, Jing Liu, Haijie Tian, Yong Li, Yongjun Bao, Zhiwei Fang, and Hanqing Lu. Dual attention network for scene segmentation. In *Proceedings of the IEEE Conference on Computer Vision and Pattern Recognition*, pages 3146–3154, 2019. 2
- [26] Leo Grady. Random walks for image segmentation. *IEEE transactions on pattern analysis and machine intelligence*, 28(11):1768–1783, 2006. 4
- [27] Varun Gulshan, Carsten Rother, Antonio Criminisi, Andrew Blake, and Andrew Zisserman. Geodesic star convexity for interactive image segmentation. In *2010 IEEE Computer Society Conference on Computer Vision and Pattern Recognition*, pages 3129–3136. IEEE, 2010. 4
- [28] Bharath Hariharan, Pablo Arbeláez, Lubomir Bourdev, Subhransu Maji, and Jitendra Malik. Semantic contours from inverse detectors. In *2011 International Conference on Computer Vision*, pages 991–998. IEEE, 2011. 4
- [29] Kaiming He, Xiangyu Zhang, Shaoqing Ren, and Jian Sun. Spatial pyramid pooling in deep convolutional networks for visual recognition. *IEEE transactions on pattern analysis and machine intelligence*, 37(9):1904–1916, 2015. 2
- [30] Kaiming He, Xiangyu Zhang, Shaoqing Ren, and Jian Sun. Deep residual learning for image recognition. In *Proceedings of the IEEE conference on computer vision and pattern recognition*, pages 770–778, 2016. 2
- [31] Seunghoon Hong, Junhyuk Oh, Honglak Lee, and Bohyung Han. Learning transferrable knowledge for semantic segmentation with deep convolutional neural network. In *Proceedings of the IEEE Conference on Computer Vision and Pattern Recognition*, pages 3204–3212, 2016. 3
- [32] Seunghoon Hong, Donghun Yeo, Suha Kwak, Honglak Lee, and Bohyung Han. Weakly supervised semantic segmentation using web-crawled videos. In *Proceedings of the IEEE Conference on Computer Vision and Pattern Recognition*, pages 7322–7330, 2017. 3
- [33] Zilong Huang, Xinggang Wang, Jiasi Wang, Wenyu Liu, and Jingdong Wang. Weakly-supervised semantic segmentation network with deep seeded region growing. In *Proceedings of the IEEE Conference on Computer Vision and Pattern Recognition*, pages 7014–7023, 2018. 3, 7
- [34] Won-Dong Jang and Chang-Su Kim. Interactive image segmentation via backpropagating refinement scheme. In *Proceedings of the IEEE Conference on Computer Vision and Pattern Recognition*, pages 5297–5306, 2019. 4
- [35] Alex Krizhevsky, Ilya Sutskever, and Geoffrey E Hinton. Imagenet classification with deep convolutional neural networks. *Advances in neural information processing systems*, 25:1097–1105, 2012. 2
- [36] Solomon Kullback and Richard A Leibler. On information and sufficiency. *The annals of mathematical statistics*, 22(1):79–86, 1951. 6
- [37] Varun Ravi Kumar, Marvin Klingner, Senthil Yogamani, Stefan Milz, Tim Fingscheidt, and Patrick Mader. Syndistnet: Self-supervised monocular fisheye camera distance estimation synergized with semantic segmentation for autonomous driving. In *Proceedings of the IEEE/CVF Winter Conference on Applications of Computer Vision (WACV)*, pages 61–71, January 2021. 1
- [38] Varun Ravi Kumar, Marvin Klingner, Senthil Yogamani, Stefan Milz, Tim Fingscheidt, and Patrick Mader. Syndistnet: Self-supervised monocular fisheye camera distance estimation synergized with semantic segmentation for autonomous driving. In *Proceedings of the IEEE/CVF Winter Conference on Applications of Computer Vision*, pages 61–71, 2021. 3
- [39] Hong Joo Lee, Jung Uk Kim, Sangmin Lee, Hak Gu Kim, and Yong Man Ro. Structure boundary preserving segmentation for medical image with ambiguous boundary. In *IEEE/CVF Conference on Computer Vision and Pattern Recognition (CVPR)*, June 2020. 1
- [40] Jungbeom Lee, Eunji Kim, Sungmin Lee, Jangho Lee, and Sungroh Yoon. Ficklenet: Weakly and semi-supervised semantic image segmentation using stochastic inference. In *Proceedings of the IEEE/CVF Conference on Computer Vision and Pattern Recognition*, pages 5267–5276, 2019. 3, 7
- [41] Matthew J. Leotta, Chengjiang Long, Bastien Jacquet, Matthieu Zins, Dan Lipsa, Jie Shan, Bo Xu, Zhixin Li, Xu Zhang, Shih-Fu Chang, Matthew Purri, Jia Xue, and Kristin Dana. Urban semantic 3d reconstruction from multiview satellite imagery. In *Proceedings of the IEEE/CVF Conference on Computer Vision and Pattern Recognition (CVPR) Workshops*, June 2019. 1
- [42] Dong Li, Jia-Bin Huang, Yali Li, Shengjin Wang, and Ming-Hsuan Yang. Weakly supervised object localization with progressive domain adaptation. In *Proceedings of the IEEE Conference on Computer Vision and Pattern Recognition*, pages 3512–3520, 2016. 2
- [43] Zhuwen Li, Qifeng Chen, and Vladlen Koltun. Interactive image segmentation with latent diversity. In *Proceedings of the IEEE Conference on Computer Vision and Pattern Recognition*, pages 577–585, 2018. 4
- [44] Orly Liba, Longqi Cai, Yun-Ta Tsai, Elad Eban, Yair Movshovitz-Attias, Yael Pritch, Huizhong Chen, and Jonathan T. Barron. Sky optimization: Semantically aware image processing of skies in low-light photography. In *Proceedings of the IEEE/CVF Conference on Computer Vision and Pattern Recognition (CVPR) Workshops*, June 2020. 1
- [45] Di Lin, Jifeng Dai, Jiaya Jia, Kaiming He, and Jian Sun. Scribblesup: Scribble-supervised convolutional networks for semantic segmentation. In *Proceedings of the IEEE Conference on Computer Vision and Pattern Recognition*, pages 3159–3167, 2016. 1
- [46] Guosheng Lin, Anton Milan, Chunhua Shen, and Ian Reid. Refinenet: Multi-path refinement networks for high-resolution semantic segmentation. In *Proceedings of the*

- IEEE Conference on Computer Vision and Pattern Recognition (CVPR)*, July 2017. 2
- [47] Tsung-Yi Lin, Piotr Dollár, Ross Girshick, Kaiming He, Bharath Hariharan, and Serge Belongie. Feature pyramid networks for object detection. In *Proceedings of the IEEE conference on computer vision and pattern recognition*, pages 2117–2125, 2017. 2
- [48] Tsung-Yi Lin, Michael Maire, Serge Belongie, James Hays, Pietro Perona, Deva Ramanan, Piotr Dollár, and C Lawrence Zitnick. Microsoft coco: Common objects in context. In *European conference on computer vision*, pages 740–755. Springer, 2014. 1
- [49] Jonathan Long, Evan Shelhamer, and Trevor Darrell. Fully convolutional networks for semantic segmentation. In *Proceedings of the IEEE conference on computer vision and pattern recognition*, pages 3431–3440, 2015. 1, 2
- [50] Ilya Loshchilov and Frank Hutter. Sgdr: Stochastic gradient descent with warm restarts. *arXiv preprint arXiv:1608.03983*, 2016. 7
- [51] Emmanuel Maggiori, Yuliya Tarabalka, Guillaume Charpiat, and Pierre Alliez. Can semantic labeling methods generalize to any city? the inria aerial image labeling benchmark. In *2017 IEEE International Geoscience and Remote Sensing Symposium (IGARSS)*, pages 3226–3229. IEEE, 2017. 6, 7, 8
- [52] Kevis-Kokitsi Maninis, Sergi Caelles, Jordi Pont-Tuset, and Luc Van Gool. Deep extreme cut: From extreme points to object segmentation. In *Proceedings of the IEEE Conference on Computer Vision and Pattern Recognition*, pages 616–625, 2018. 4
- [53] Gregory P. Meyer, Jake Charland, Darshan Hegde, Ankit Laddha, and Carlos Vallespi-Gonzalez. Sensor fusion for joint 3d object detection and semantic segmentation. In *Proceedings of the IEEE/CVF Conference on Computer Vision and Pattern Recognition (CVPR) Workshops*, June 2019. 1
- [54] Josh Myers-Dean and Scott Wehrwein. Semantic pixel distances for image editing. In *Proceedings of the IEEE/CVF Conference on Computer Vision and Pattern Recognition (CVPR) Workshops*, June 2020. 1
- [55] Maxime Oquab, Leon Bottou, Ivan Laptev, and Josef Sivic. Is object localization for free? - weakly-supervised learning with convolutional neural networks. In *Proceedings of the IEEE Conference on Computer Vision and Pattern Recognition (CVPR)*, June 2015. 1, 2, 3, 7
- [56] George Papandreou, Liang-Chieh Chen, Kevin P Murphy, and Alan L Yuille. Weakly-and semi-supervised learning of a deep convolutional network for semantic image segmentation. In *Proceedings of the IEEE international conference on computer vision*, pages 1742–1750, 2015. 3, 7
- [57] Adam Paszke, Sam Gross, Francisco Massa, Adam Lerer, James Bradbury, Gregory Chanan, Trevor Killeen, Zeming Lin, Natalia Gimelshein, Luca Antiga, Alban Desmaison, Andreas Kopf, Edward Yang, Zachary DeVito, Martin Raison, Alykhan Tejani, Sasank Chilamkurthy, Benoit Steiner, Lu Fang, Junjie Bai, and Soumith Chintala. Pytorch: An imperative style, high-performance deep learning library. In H. Wallach, H. Larochelle, A. Beygelzimer, F. d'Alché-Buc, E. Fox, and R. Garnett, editors, *Advances in Neural Information Processing Systems 32*, pages 8024–8035. Curran Associates, Inc., 2019. 1
- [58] Pedro O Pinheiro and Ronan Collobert. From image-level to pixel-level labeling with convolutional networks. In *Proceedings of the IEEE conference on computer vision and pattern recognition*, pages 1713–1721, 2015. 1, 3, 7
- [59] Siyuan Qiao, Huiyu Wang, Chenxi Liu, Wei Shen, and Alan Yuille. Weight standardization. *arXiv preprint arXiv:1903.10520*, 2019. 7
- [60] Vinicius Ribeiro, Sandra Avila, and Eduardo Valle. Less is more: Sample selection and label conditioning improve skin lesion segmentation. In *Proceedings of the IEEE/CVF Conference on Computer Vision and Pattern Recognition (CVPR) Workshops*, June 2020. 1
- [61] Olaf Ronneberger, Philipp Fischer, and Thomas Brox. U-net: Convolutional networks for biomedical image segmentation. In *International Conference on Medical image computing and computer-assisted intervention*, pages 234–241. Springer, 2015. 1, 2
- [62] Carsten Rother, Vladimir Kolmogorov, and Andrew Blake. ” grabcut” interactive foreground extraction using iterated graph cuts. *ACM transactions on graphics (TOG)*, 23(3):309–314, 2004. 4
- [63] Anirban Roy and Sinisa Todorovic. Combining bottom-up, top-down, and smoothness cues for weakly supervised image segmentation. In *Proceedings of the IEEE Conference on Computer Vision and Pattern Recognition*, pages 3529–3538, 2017. 3, 7
- [64] Ramprasaath R Selvaraju, Michael Cogswell, Abhishek Das, Ramakrishna Vedantam, Devi Parikh, and Dhruv Batra. Grad-cam: Visual explanations from deep networks via gradient-based localization. In *Proceedings of the IEEE international conference on computer vision*, pages 618–626, 2017. 1, 2, 3, 7
- [65] Wataru Shimoda and Keiji Yanai. Self-supervised difference detection for weakly-supervised semantic segmentation. In *Proceedings of the IEEE/CVF International Conference on Computer Vision*, pages 5208–5217, 2019. 3, 7
- [66] Karen Simonyan and Andrew Zisserman. Very deep convolutional networks for large-scale image recognition. *arXiv preprint arXiv:1409.1556*, 2014. 2
- [67] Thomas J. Smith, Michel Valstar, Don Sharkey, and John Crowe. Clinical scene segmentation with tiny datasets. In *Proceedings of the IEEE/CVF International Conference on Computer Vision (ICCV) Workshops*, Oct 2019. 1
- [68] Hang Su, Varun Jampani, Deqing Sun, Orazio Gallo, Erik Learned-Miller, and Jan Kautz. Pixel-adaptive convolutional neural networks. In *Proceedings of the IEEE/CVF Conference on Computer Vision and Pattern Recognition*, pages 11166–11175, 2019. 3
- [69] Christian Szegedy, Wei Liu, Yangqing Jia, Pierre Sermanet, Scott Reed, Dragomir Anguelov, Dumitru Erhan, Vincent Vanhoucke, and Andrew Rabinovich. Going deeper with convolutions. In *Proceedings of the IEEE conference on computer vision and pattern recognition*, pages 1–9, 2015. 2

- [70] Yuxing Tang, Josiah Wang, Boyang Gao, Emmanuel Delandrea, Robert Gaizauskas, and Liming Chen. Large scale semi-supervised object detection using visual and semantic knowledge transfer. In *Proceedings of the IEEE Conference on Computer Vision and Pattern Recognition*, pages 2119–2128, 2016. [2](#)
- [71] Stefanie Tanujaya, Tieh Chu, Jia-Hao Liu, and Wen-Hsiao Peng. Semantic segmentation on compressed video using block motion compensation and guided inpainting. In *2020 IEEE International Symposium on Circuits and Systems (IS-CAS)*, pages 1–5. IEEE, 2020. [3](#)
- [72] Serin Varghese, Yasin Bayzidi, Andreas Bar, Nikhil Kapoor, Sounak Lahiri, Jan David Schneider, Nico M. Schmidt, Peter Schlicht, Fabian Huger, and Tim Fingscheidt. Unsupervised temporal consistency metric for video segmentation in highly-automated driving. In *Proceedings of the IEEE/CVF Conference on Computer Vision and Pattern Recognition (CVPR) Workshops*, June 2020. [1](#)
- [73] Shuxin Wang, Shilei Cao, Dong Wei, Renzhen Wang, Kai Ma, Liansheng Wang, Deyu Meng, and Yefeng Zheng. Lt-net: Label transfer by learning reversible voxel-wise correspondence for one-shot medical image segmentation. In *IEEE/CVF Conference on Computer Vision and Pattern Recognition (CVPR)*, June 2020. [1](#), [2](#), [3](#)
- [74] Xiang Wang, Shaodi You, Xi Li, and Huimin Ma. Weakly-supervised semantic segmentation by iteratively mining common object features. In *Proceedings of the IEEE conference on computer vision and pattern recognition*, pages 1354–1362, 2018. [7](#)
- [75] Yude Wang, Jie Zhang, Meina Kan, Shiguang Shan, and Xilin Chen. Self-supervised equivariant attention mechanism for weakly supervised semantic segmentation. In *Proceedings of the IEEE/CVF Conference on Computer Vision and Pattern Recognition*, pages 12275–12284, 2020. [2](#), [3](#), [7](#)
- [76] Anne S Wannenwetsch and Stefan Roth. Probabilistic pixel-adaptive refinement networks. In *Proceedings of the IEEE/CVF Conference on Computer Vision and Pattern Recognition*, pages 11642–11651, 2020. [3](#)
- [77] Yunchao Wei, Huaxin Xiao, Honghui Shi, Zequn Jie, Jiashi Feng, and Thomas S Huang. Revisiting dilated convolution: A simple approach for weakly-and semi-supervised semantic segmentation. In *Proceedings of the IEEE Conference on Computer Vision and Pattern Recognition*, pages 7268–7277, 2018. [7](#)
- [78] Yuxin Wu and Kaiming He. Group normalization. In *Proceedings of the European conference on computer vision (ECCV)*, pages 3–19, 2018. [7](#)
- [79] Zifeng Wu, Chunhua Shen, and Anton Van Den Hengel. Wider or deeper: Revisiting the resnet model for visual recognition. *Pattern Recognition*, 90:119–133, 2019. [1](#), [7](#)
- [80] Ning Xu, Brian Price, Scott Cohen, Jimei Yang, and Thomas S Huang. Deep interactive object selection. In *Proceedings of the IEEE Conference on Computer Vision and Pattern Recognition*, pages 373–381, 2016. [4](#)
- [81] Xiangyu Xu, Yongrui Ma, and Wenxiu Sun. Learning factorized weight matrix for joint filtering. In *International Conference on Machine Learning*, pages 10587–10596. PMLR, 2020. [3](#)
- [82] Qihang Yu, Dong Yang, Holger Roth, Yutong Bai, Yixiao Zhang, Alan L. Yuille, and Daguang Xu. C2fnas: Coarse-to-fine neural architecture search for 3d medical image segmentation. In *IEEE/CVF Conference on Computer Vision and Pattern Recognition (CVPR)*, June 2020. [1](#)
- [83] Hang Zhang, Kristin Dana, Jianping Shi, Zhongyue Zhang, Xiaogang Wang, Amrith Tyagi, and Amit Agrawal. Context encoding for semantic segmentation. In *Proceedings of the IEEE conference on Computer Vision and Pattern Recognition*, pages 7151–7160, 2018. [1](#), [2](#)
- [84] Shanshan Zhang, Rodrigo Benenson, and Bernt Schiele. Citypersons: A diverse dataset for pedestrian detection. In *CVPR*, 2017. [6](#), [7](#), [8](#)
- [85] Hengshuang Zhao, Jianping Shi, Xiaojuan Qi, Xiaogang Wang, and Jiaya Jia. Pyramid scene parsing network. In *Proceedings of the IEEE conference on computer vision and pattern recognition*, pages 2881–2890, 2017. [1](#), [2](#)
- [86] Bolei Zhou, Aditya Khosla, Agata Lapedriza, Aude Oliva, and Antonio Torralba. Learning deep features for discriminative localization. In *Proceedings of the IEEE conference on computer vision and pattern recognition*, pages 2921–2929, 2016. [1](#), [2](#), [7](#)
- [87] Bolei Zhou, Hang Zhao, Xavier Puig, Sanja Fidler, Adela Barriuso, and Antonio Torralba. Scene parsing through ade20k dataset. In *Proceedings of the IEEE Conference on Computer Vision and Pattern Recognition*, 2017. [1](#)
- [88] Dingfu Zhou, Jin Fang, Xibin Song, Liu Liu, Junbo Yin, Yuchao Dai, Hongdong Li, and Ruigang Yang. Joint 3d instance segmentation and object detection for autonomous driving. In *IEEE/CVF Conference on Computer Vision and Pattern Recognition (CVPR)*, June 2020. [1](#)
- [89] Yanzhao Zhou, Yi Zhu, Qixiang Ye, Qiang Qiu, and Jianbin Jiao. Weakly supervised instance segmentation using class peak response. In *Proceedings of the IEEE Conference on Computer Vision and Pattern Recognition*, pages 3791–3800, 2018. [1](#), [2](#), [3](#), [8](#)